

Crystal structure of the adenosine A_{2A} receptor bound to an antagonist reveals a potential allosteric pocket

Bingfa Sun^a, Priti Bachhawat^a, Matthew Ling-Hon Chu^a, Martyn Wood^b, Tom Ceska^c, Zara A. Sands^d, Joel Mercier^d, Florence Lebon^d, Tong Sun Kobilka^a, and Brian K. Kobilka^{a,e,1}

^aConfometRx, Inc., Santa Clara, CA 95054; ^bDiscovery Biology, New Medicines, UCB Pharma, B-1420 Braine-l'Alleud, Belgium; ^cDepartment of Structural Biology, New Medicines, UCB Pharma, Slough SL1 3WE, United Kingdom; ^dDiscovery Chemistry, New Medicines, UCB Pharma, B-1420 Braine-l'Alleud, Belgium and ^eDepartment of Molecular and Cellular Physiology, Stanford University School of Medicine, Stanford, CA 94305

Contributed by Brian K. Kobilka, December 29, 2016 (sent for review October 17, 2016; reviewed by Oliver P. Ernst and Nagarajan Vaidehi)

The adenosine A_{2A} receptor (A_{2A}R) has long been implicated in cardiovascular disorders. As more selective A_{2A}R ligands are being identified, its roles in other disorders, such as Parkinson's disease, are starting to emerge, and A_{2A}R antagonists are important drug candidates for nondopaminergic anti-Parkinson treatment. Here we report the crystal structure of A_{2A} receptor bound to compound 1 (Cmpd-1), a novel A_{2A}R/*N*-methyl *D*-aspartate receptor subtype 2B (NR2B) dual antagonist and potential anti-Parkinson candidate compound, at 3.5 Å resolution. The A_{2A} receptor with a cytochrome b562-RIL (BRIL) fusion (A_{2A}R-BRIL) in the intracellular loop 3 (ICL3) was crystallized in detergent micelles using vapor-phase diffusion. Whereas A_{2A}R-BRIL bound to the antagonist ZM241385 has previously been crystallized in lipidic cubic phase (LCP), structural differences in the Cmpd-1-bound A_{2A}R-BRIL prevented formation of the lattice observed with the ZM241385-bound receptor. The crystals grew with a type II crystal lattice in contrast to the typical type I packing seen from membrane protein structures crystallized in LCP. Cmpd-1 binds in a position that overlaps with the native ligand adenosine, but its methoxyphenyl group extends to an exosite not previously observed in other A_{2A}R structures. Structural analysis revealed that Cmpd-1 binding results in the unique conformations of two tyrosine residues, Tyr9^{1,35} and Tyr271^{7,36}, which are critical for the formation of the exosite. The structure reveals insights into antagonist binding that are not observed in other A_{2A}R structures, highlighting flexibility in the binding pocket that may facilitate the development of A_{2A}R-selective compounds for the treatment of Parkinson's disease.

GPCR | A_{2A} adenosine receptor | structure | allosteric | Parkinson's disease

The adenosine A_{2A} receptor (A_{2A}R) is one of the four subtypes of adenosine receptors (A₁R, A_{2A}R, A_{2B}R, A₃R). As a member of the G protein-coupled receptor (GPCR) family, the A_{2A} receptor couples to stimulatory G protein G_s and elevates intracellular cAMP upon activation by endogenous adenosine. The A_{2A}R has been an attractive drug target due to its role in cardiovascular and immune system function, as well as in the central nervous system as a potential therapeutic target for Parkinson's disease (PD) (1–4). PD is a neurodegenerative disease that affects more than 1% of the population over 65 years old. Currently, major treatments target the restoration of dopamine signaling, which is impaired in PD patients, by dopamine-replacing agents. Although these treatments effectively address PD-related motor disturbances, the long-term use of dopamine-replacing agents is associated with the development of motor complications; therefore, there is a need for nondopaminergic drugs (2). It is known that A_{2A}R signaling regulates dopaminergic neurotransmission, and A_{2A}R antagonists have been shown to enhance D2 dopamine receptor signaling, which has been found to improve PD symptoms in animal models and patients, without the side effects common to dopamine-replacing agents, such as dyskinesia (1, 5). Therefore, A_{2A}R antagonists are good candidates for nondopaminergic treatment of PD. A more recent study found combined administration of A_{2A}R and *N*-methyl *D*-aspartate receptor subtype 2B (NR2B) antagonists significantly improved motor activity, and the effects were sustained

for longer than when administered separately at the same dose in a rodent model of PD (6). In an effort to identify a dual compound displaying A_{2A}R as well as NR2B receptor antagonist activities, Cmpd-1 was designed and synthesized. The compound binds to both receptors with high affinity (Table 1). To understand the structure–activity relationship around the chemical series for the A_{2A}R and facilitate further optimization, we sought to obtain the crystal structure of the A_{2A}R in complex with Cmpd-1. Although a number of crystal structures of A_{2A}R bound to various antagonists and agonists have been reported (7–14) using lipidic cubic phase (LCP) methods (15, 16), we were unable to obtain high-quality crystals of A_{2A}R bound to Cmpd-1. As an alternative approach we obtained a 3.5-Å resolution crystal structure of A_{2A}R in complex with Cmpd-1 by using a BRIL fusion construct and performing the crystallization in vapor-phase diffusion in the detergent lauryl maltose neopentyl glycol (LMNG). This structure of a nonrhodopsin GPCR was obtained in a detergent environment without thermostabilizing mutations or antibody fragment. Structural analysis provides insight into the binding mode of Cmpd-1 and reveals a potential allosteric pocket that is not observed in previously reported A_{2A}R structures. The structural information provides a rationale for the higher affinity of Cmpd-1 compared with its closely related analogs.

Results and Discussion

Cmpd-1, a Novel Potential Anti-Parkinson Candidate. We identified a unique molecule, referred to as Cmpd-1 (Fig. 1A), that behaves

Significance

The A_{2A}R is a G protein-coupled receptor (GPCR) that plays important roles in cardiovascular physiology and immune function. The A_{2A}R is also a target for the treatment of Parkinson's disease, where A_{2A}R antagonists have been shown to enhance signaling through the D2 dopamine receptor. Here we present the crystal structure of the A_{2A}R bound to a novel bitopic antagonist. As a result of structural changes needed to accommodate the bound antagonist, crystals could not be grown in lipidic cubic phase. Instead, crystals were grown in detergent with a type II packing rarely observed in GPCR crystals. The structure revealed a potential allosteric pocket that can be exploited to develop subtype-selective allosteric modulators.

Author contributions: B.S., F.L., T.S.K., and B.K.K. designed research; B.S., P.B., M.L.-H.C., M.W., T.C., Z.A.S., J.M., and F.L. performed research; B.S., Z.A.S., F.L., and B.K.K. analyzed data; and B.S. and B.K.K. wrote the paper.

Reviewers: O.P.E., University of Toronto; and N.V., Beckman Research Institute of the City of Hope.

Conflict of interest statement: The research was performed by ConfometRx, Inc., founded by T.S.K. and B.K.K., in collaboration with UCB Pharma.

Freely available online through the PNAS open access option.

Data deposition: The atomic coordinates and structure factors have been deposited in the Protein Data Bank, www.pdb.org (PDB ID code 5UIG).

¹To whom correspondence should be addressed. Email: kobilka@stanford.edu.

This article contains supporting information online at www.pnas.org/lookup/suppl/doi:10.1073/pnas.1621423114/-DCSupplemental.

Table 1. Binding properties of Cmpd-1 to A_{2A}R, A₁, and NR2B receptors

Receptor	pKi*	n**	Radioligand
A _{2A}	7.95 ± 0.06	4	[³ H]-ZM241385
A ₁	6.8	2	[³ H]-DPCPX
NR2B	8.25 ± 0.17	4	[³ H]-UCB9352***

*Negative logarithm of the equilibrium dissociation constant of Cmpd-1 determined by competitive binding assay.

**Number of parallel tests for the binding assay.

***Proprietary compound of UCB.

as an A_{2A}R/NR2B dual antagonist. Cmpd-1 has a 15-fold higher affinity for the A_{2A}R than the A₁R (with pKi values of 7.95 and 6.8, respectively; Table 1) and binds NR2B with high affinity (pKi = 8.25); it functions as an A_{2A}R antagonist able to block CGS21680-induced A_{2A} receptor activation with pK_b 7.00 ± 0.32 (*n* = 4). Cmpd-1 contains three rings: methylphenyl, aminotriazole, and orthomethoxyphenyl (Fig. 1A). We synthesized and tested close analogs of Cmpd-1 where the orthomethoxyphenyl group was replaced by different R groups (Table 2). The results revealed that migration of the methoxy group around the ring, or removal of the methoxy group, reduced the affinity significantly for A_{2A}R but not for A₁R, whereas replacement of methoxyphenyl with a cyclopropyl ring reduced the affinity for both receptors. Our efforts to dock Cmpd-1 into previously reported A_{2A}R structures could not help us to rationalize affinity-boosting effects associated with the orthomethoxyphenyl R group. Therefore, to help facilitate further optimization efforts around this chemotype we sought to obtain a crystal structure of A_{2A}R in complex with Cmpd-1 to provide much-needed insight into the binding mode of this lead molecule.

Crystallization of A_{2A}R in Complex with Cmpd-1. The LCP method for membrane protein crystallography (15, 16) has been used successfully to crystallize a number of GPCRs over the past several years and has become the method of choice; this is exemplified by the fact that 38 of the 39 GPCRs with structures reported have been successfully crystallized in LCP. Therefore, we initially attempted to crystallize A_{2A}R in complex with Cmpd-1 in LCP. We started our trials in LCP using a construct with T4 lysozyme (T4L) inserted into the intracellular loop 3 (ICL3) of A_{2A}R (A_{2A}R–T4L) as previously reported (14). We were able to obtain crystals of A_{2A}R–T4L bound to Cmpd-1 in LCP with comparable size and shape to those previously described (14). However, we were unable to optimize the crystal to diffract beyond 5 Å. As an alternative, we replaced T4L with a truncated modified T4L (mT4L), which has a deleted small lobe of T4L and has previously helped to improve diffraction of muscarinic M3 receptor crystals (17). We obtained slightly improved crystals and obtained a dataset at 4.6 Å resolution. Although the structure could be solved by molecular replacement, the electron density map showed no density to model the ligand (Fig. S1). We noted that the packing of this crystal lattice is not as tight as the packing in the reported A_{2A}R–T4L or A_{2A}R–BRIL crystals (Fig. S1), resulting in higher solvent content, and postulated that this may have contributed to the poorer diffraction. Insertion of thermostabilized apocytochrome b562RIL (BRIL) into ICL3 of A_{2A}R was reported to improve the thermostability of the fusion protein (A_{2A}R–BRIL), and crystals of A_{2A}R–BRIL were obtained in LCP and diffracted to 1.8 Å (8, 18). However, despite extensive crystallization trials, we were not able to obtain any crystals of A_{2A}R–BRIL bound to Cmpd-1 or its analogs in LCP. As a control experiment, we reproduced the crystals of A_{2A}R–BRIL in complex with ZM241385 using previously reported conditions (8), and the crystals diffracted well beyond 2.0 Å

resolution with one trial, indicating the protein preparation and methods used were adequate.

It is now widely understood that the key to successful crystallization of a GPCR is to maintain its conformational homogeneity. The bound ligand is critical in stabilizing a GPCR in a certain conformation, and if the ligand rapidly binds and dissociates due to its low affinity, the receptor will likely adopt multiple conformations that impair the crystallization process. The affinity of Cmpd-1 is ~10- to 20-fold weaker than ZM241385 (14), and this difference could also be detrimental to crystallization efforts.

We finally obtained crystals of A_{2A}R–BRIL in complex with Cmpd-1 by vapor diffusion with the receptor present in the detergent LMNG. This was surprising because all previously reported crystal structures of nonthermostabilized GPCRs with a fusion partner have been solved using LCP, and not vapor diffusion crystallization. Initial crystal hits were obtained through screening in commercial broad screens for membrane proteins and, after optimization, a 3.5-Å resolution data set was obtained by combining diffraction data from 20 crystals (Fig. S2). The structure was solved by molecular replacement and the quality of the electron density maps was very good for this resolution (statistics in Table S1). All residues and Cmpd-1 were well defined, with the exception of residues 1–3 at N terminus, residues 149–158 on extracellular loop 2 (ECL2), and residues 312–316 located at the C terminus that could not be modeled due to weak density. A_{2A}R–BRIL is packed in the crystal lattice with a P4₁2₁2 space group (Fig. 1B), representing type II crystal packing (Fig. 1C) (19), which is rarely observed for GPCRs. It is believed that type I packing is favored for GPCRs because the detergent micelle limits packing interactions that involve the transmembrane segments. In this lattice, with one molecule in the asymmetric unit, two adjacent receptors are packed against each other to form

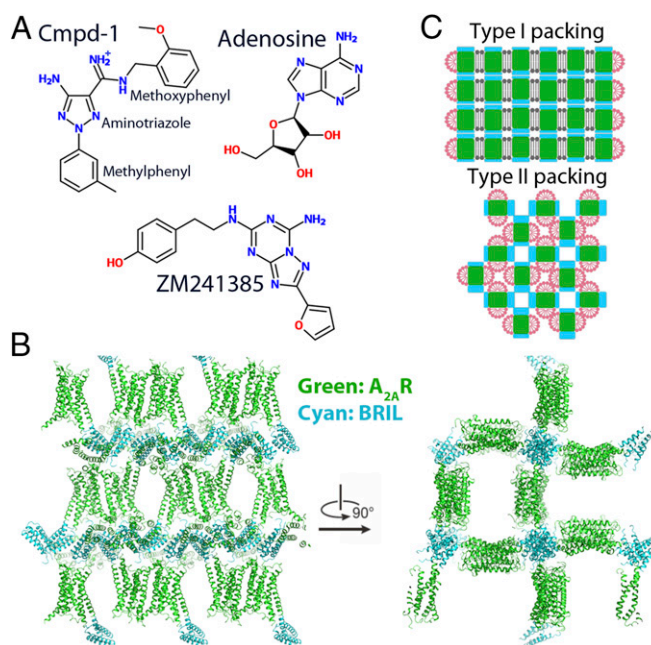
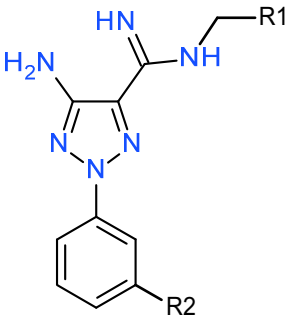


Fig. 1. Cmpd-1 chemical structure and A_{2A}R–BRIL–Cmpd-1 crystal packing. (A) Chemical structure of several A_{2A}R ligands, including Cmpd-1, ZM241385, and endogenous ligand adenosine. Cmpd-1 is predicted to be protonated under physiological pH. (B) Crystal packing of the A_{2A}R–BRIL–Cmpd-1 structure represents an unusual type II crystal packing for a GPCR. The receptor is shown in green, and BRIL is shown in cyan. (C) Schemes of type I and type II packing for membrane protein crystals. Detergent and lipid molecules are shown in pink and gray, respectively. Transmembrane segments and polar region of the membrane protein are shown in green and cyan, respectively.

Table 2. Binding properties of Cmpd-1 analogs to A_{2A} and A₁ receptors



Compound	R1	R2	A _{2A} R pKi*	A ₁ R pKi*
1	Orthomethoxyphenyl	Methyl	8.0	6.8
2	Metamethoxyphenyl	Methyl	6.8	6.6
3	Paramethoxyphenyl	Methyl	5.9	6.6
4	Phenyl	H	6.9	7.1
5	Cyclopropyl	Methyl	5.8	6.0

*Negative logarithm of the equilibrium dissociation constant of compound *x* determined by competitive binding assay. The values are the means of 2–4 independent determinations.

an antiparallel dimer through their transmembrane helix 1 (TM1), TM2, and Helix 8. Another adjacent A_{2A}R–BRIL molecule is packed with its direction pointing 90° away along the crystallographic 4₁ screw axis in the lattice, mostly through extensive interaction among BRILs. BRIL also interacts with the Helix 8 and ECL3 of the receptor. Overall, most hydrophilic crystal contacts are mediated by BRIL, as is the case for all of the GPCRs crystallized with a fusion partner.

Structure of Cmpd-1-Bound A_{2A}R–BRIL. The overall structure of A_{2A}R–Cmpd-1 is similar to other reported structures of A_{2A}R in complex with antagonists (8–10, 12, 14). For example, our structure has an rmsd of 1.1 Å and 1.4 Å over 240 Cαs when aligned with A_{2A}R–BRIL–ZM241385 structure (antagonist bound; PDB ID code 4E1Y; Fig. 2A) and A_{2A}R–T4L–UK-432097 (agonist bound, PDB ID code 3QAK) (11), respectively. Our structure represents an inactive state structure of the receptor based on the conformation of TM6, and conserved motifs such as E/DRY and NPXXY are virtually identical to that in A_{2A}R–BRIL–ZM241385 structure (8). Nevertheless, our structure has notable differences compared with the reported structure of A_{2A}R–BRIL–ZM241385, even though the crystals were generated from the same fusion protein. Some of these differences can be attributed to crystal packing, whereas others are most likely due to differences arising from interactions with the bound ligand.

The first difference can be found at the cytoplasmic end of TM5, which showed an ~8-Å outward movement comparing to its position in A_{2A}R–BRIL–ZM241385 structure (Fig. 2B) at the Cα carbon of Gln207^{5,69} (superscripts indicate Ballesteros–Weinstein numbers) (20). We cannot attribute this difference to any difference in the ligand binding pocket, and the difference may result indirectly from crystal packing, because TM5 is fused to BRIL and/or it may reflect the intrinsic flexibility of the receptor. It is noteworthy that in a thermostabilized A_{2A}R bound to the xanthine XAC (A_{2A}R–TS–XAC), Glu228^{6,30} forms an ionic interaction with Arg102^{3,50} in A_{2A}R (12) that was first observed in rhodopsin (21) and has also been observed in the D3 dopamine receptor (22). This interaction, called the ionic lock, is expected to stabilize the inactive state. In contrast, in our structure, Glu228^{6,30} forms an ionic interaction with Arg107^{3,55} with a distance of 4.0 Å (Fig. 2C), which would also stabilize the inactive conformation of TM6. This interaction between Glu228^{6,30}

and Arg107^{3,55} cannot be formed in A_{2A}R–BRIL–ZM241385 because of the position of TM5, and it is not possible in A_{2A}R–TS–XAC because Arg107^{3,55} was mutated to Ala. The second difference relates to the conformation of Helix 8 (Fig. 2A). Unlike the straight helix observed in the A_{2A}R–BRIL–ZM241385 structure, Helix 8 in our structure has a kink starting from Gln297. Because this part of Helix 8 is extensively involved in crystal contacts (Fig. 1B), this difference is likely caused by crystal packing. The third difference pertains to the location of the Cα atom of Met4^{1,30} toward the extracellular end of TM1, which is ~4 Å further from the TM core than in the A_{2A}R–BRIL–ZM241385 structure (Fig. 2D). This difference, albeit more subtle in comparison with the first two, is most likely caused by the binding of Cmpd-1 and may explain the reason for not obtaining the same crystal packing as A_{2A}R–BRIL–ZM241385 in LCP; this will be discussed in more detail below.

It should be noted that electron density provided evidence for an alternate conformation for ECL2 in our structure involving Phe168 and, to a lesser extent, Leu167 and Glu169. The side chain of Phe168 adopts two very different conformations (Fig. S3). According to the density map and refinement results, the conformation in which the side chain of Phe168 projects into the receptor core and makes π–π interaction with the ligand seems to be the dominant conformation at occupancy of 0.7, which is consistent with its conformation in all other reported A_{2A}R structures (7–14). Further discussion of the binding pocket will be based on this single conformation.

Cmpd-1 Binding Pocket. Cmpd-1 is well defined in the density map (Fig. 3A). The closely linked methylphenyl and aminotriazole rings occupy similar positions as the furan ring and triazolotriazine core of ZM241385, respectively (Fig. S4) (8, 10, 12, 14); in this deep pocket, they make extensive hydrophobic interactions and form hydrogen bonds with surrounding residues (Fig. 3B). Some interactions are common among various A_{2A}R ligands: the amide nitrogen of Asn253^{6,55} makes a hydrogen bond with a nitrogen atom on the aminotriazole ring, and Phe168 on ECL2 makes aromatic stacking interaction with the aminotriazole ring. These two residues also make critical interactions

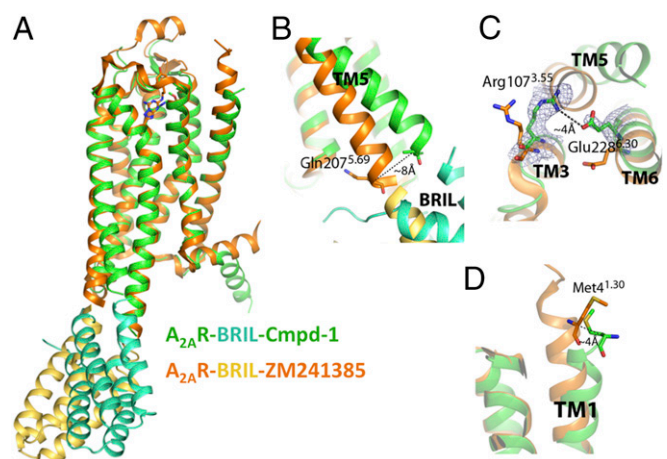


Fig. 2. Structure features of A_{2A}R–BRIL in complex with Cmpd-1. (A) Overall structure comparison of A_{2A}R–BRIL–Cmpd-1 (receptor and ligand in green; BRIL in cyan) and A_{2A}R–BRIL–ZM241385 (receptor and ligand in orange; BRIL in gold). (B) Structural comparison of the intracellular part of TM5. In the A_{2A}R–BRIL–Cmpd-1 structure, TM5 is displaced by 8 Å at the Cα of Gln207^{5,69} relative to the A_{2A}R–BRIL–ZM241385 structure. (C) In the A_{2A}R–BRIL–Cmpd-1 structure, Glu228^{6,30} forms a salt bridge with Arg107^{3,55}, which is only possible because of the displacement of TM5 noted above. The map is 2F_o–F_c map contoured at 1.5 σ. (D) Structural comparison of the N-terminal aspect of the TM1 helices between the two structures where the Cα atoms of Met4^{1,30} are ~4 Å apart.

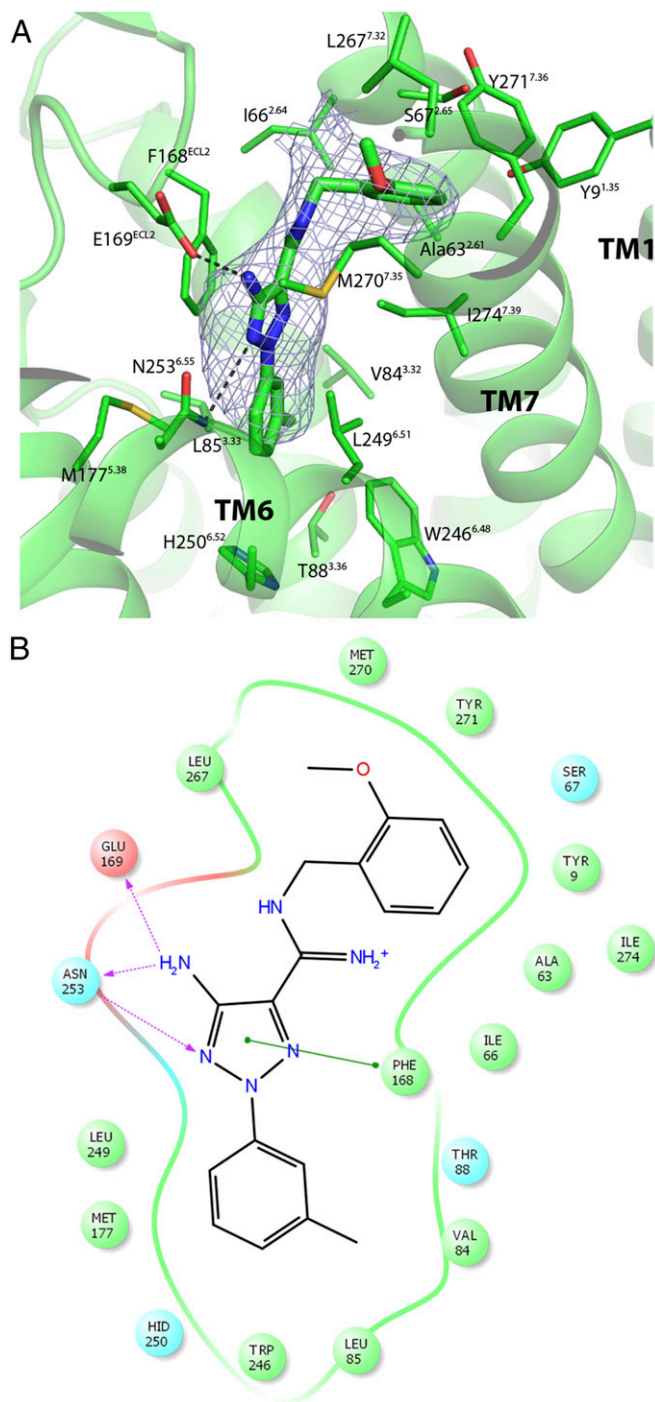


Fig. 3. Binding interactions between the $A_{2A}R$ and Cmpd-1. (A) Cmpd-1 binding pocket. The side chains of residues within 4 Å of the ligand are shown in stick. Hydrogen bonding interactions are depicted with dashed lines. The $F_o - F_c$ omit map around the ligand is shown as mesh contoured at 2.5 σ . (B) A schematic representation of Cmpd-1 binding interactions. The residues within 4 Å of Cmpd-1 are shown as spheres, with polar, hydrophobic, and negatively charged residues colored cyan, green, and red, respectively. The π - π stacking interaction of the aminotriazole ring with Phe168 is depicted with a solid green line. The hydrogen bonding interactions with the side chains of Asn253 and Glu169 are depicted with dotted pink lines. The protein pocket is displayed with a line around the ligand, colored according to the nearest residue. A gap in the line shows an opening in the pocket, and the minimum gap observed in this diagram indicates that Cmpd-1 is very well buried. The iminium of Cmpd-1 and His250 are predicted to be protonated due to the low pH (6.5) of crystallization conditions.

with $A_{2A}R$ ligands in all reported $A_{2A}R$ structures. In addition, Glu169 on ECL2 forms a hydrogen bond to the amine group of the aminotriazole ring, and it also interacts with adenosine by forming a hydrogen bond. Overall, the methylphenyl and aminotriazole groups bind within the orthosteric pocket of $A_{2A}R$, as defined by the space occupied by adenosine (Fig. S4) (13).

The methoxyphenyl ring of Cmpd-1 extends to an adjacent and previously unobserved binding pocket formed by Tyr⁹^{1.35}, Ala63^{2.61}, Ile66^{2.64}, Ser67^{2.65}, Leu267^{7.32}, Met270^{7.35}, Tyr271^{7.36}, and Ile274^{7.39}, toward the extracellular aspect of TM1, TM2, and TM7 (Fig. 3); this is different from the binding mode of ZM241385 in $A_{2A}R$ -BRIL, which has its phenol ring extended toward solvent-exposed surface, but is somewhat reminiscent of its binding mode in thermostabilized $A_{2A}R$ (Fig. 4A) (8). Among the surrounding residues, Tyr⁹^{1.35} and Tyr271^{7.36} make key aromatic interactions with Cmpd-1's phenyl ring, and their positions and rotamers are unique compared with other reported $A_{2A}R$ structures (Fig. 4A and Fig. S5) (7–14). Specifically, Tyr⁹^{1.35} moves 1.7 Å away from the TM core (Fig. 4A) compared with its position in $A_{2A}R$ -BRIL-ZM241385 structure, to enable the receptor to accommodate the methoxyphenyl moiety. The difference in the position of Tyr⁹^{1.35} is amplified at the extracellular end of TM1 (C α of Met4^{1.30}) to \sim 4 Å. In the $A_{2A}R$ -BRIL-ZM241385 crystal lattice, the extracellular end of TM1 makes important crystal lattice contacts with an adjacent symmetry-related molecule, and the position of TM1 observed in our structure is incompatible with this packing (Fig. S6) (8), which may explain why we failed to crystallize $A_{2A}R$ -BRIL-Cmpd-1 in the same lattice form as observed for $A_{2A}R$ -BRIL-ZM241385 in LCP. The other aromatic residue Tyr271^{7.36} effectively covers the methoxyphenyl group and prevents it from becoming directly exposed to the solvent by adopting a rotamer very different from that found in the structures of $A_{2A}R$ -BRIL or thermostabilized $A_{2A}R$ bound to ZM241385 (Fig. 4A and Fig. S5) (12). The dramatic loss of potency observed upon replacement of the methoxyphenyl with cyclopropyl indicates the critical importance of aromatic interactions for Cmpd-1 binding (Table 2). In comparison, substitution of the phenol ring of ZM241385 with a cycloalkyl group did not alter the affinity for $A_{2A}R$ significantly (23), consistent with the reported structures that the phenol ring is primarily making hydrophobic interactions with $A_{2A}R$ (PDB ID code 3PWH), or primarily solvent exposed (PDB ID code 4E1Y) (12, 14).

As a result of the unique conformations of these two aromatic residues, a relatively compact pocket is formed in our structure that accommodates the methoxyphenyl ring (Fig. 4B and Fig. S7), whereas the equivalent part in other reported $A_{2A}R$ structures is either very shallow (i.e., in $A_{2A}R$ -BRIL-ZM241385) (8) or more exposed to solvent as a cleft (i.e., in $A_{2A}R$ -TS-ZM241385) (12) (Fig. S7). The methoxyphenyl ring of Cmpd-1 has lower B-factors (averaged at 78.1 Å²) than the whole ligand (averaged at 93.9 Å²), suggesting that binding within this pocket stabilizes its position in the crystal. The eight residues that form this pocket tightly surround the methoxyphenyl R group of Cmpd-1 (Fig. 4B and Fig. S7), and leave no additional space for accommodating this ring with a methoxy group in either the meta or para position. Specifically, metamethoxyphenyl substitution will cause steric clash with Tyr271^{7.36}, or Ala63^{2.61}, Tyr⁹^{1.35}, Ile66^{2.64}, whereas paramethoxyphenyl substitution will cause steric clash with Tyr⁹^{1.35}, and Ala63^{2.61} or Tyr271^{7.36}, depending on the rotamers of the methoxyphenyl ring. This binding mode is consistent with the results that meta- and paramethoxy analogs of the Cmpd-1 have significantly lower affinity for $A_{2A}R$ (Table 2).

Because the native ligand adenosine does not extend to this pocket, it may represent a potential allosteric site that would not be predicted from other reported $A_{2A}R$ structures. Binding results also suggest that the binding interactions in this pocket are critical for the selectivity of Cmpd-1 for $A_{2A}R$ over A_1R , because modifications of the orthomethoxyphenyl ring result in loss of selectivity between $A_{2A}R$ and A_1R (Table 2). Sequence alignment showed

37,800 × g. Extraction of A_{2A} receptor from Sf9 membranes was done with a Dounce homogenizer in a solubilization buffer comprised of 1% *n*-dodecyl β-D-maltoside (DDM), 0.03% cholesteryl hemisuccinate (CHS), 30 mM Hepes, pH 7.8, 800 mM NaCl, 30% (vol/vol) glycerol, 2 mg/mL iodoacetamide, 2.5 μg/mL leupeptin, 0.16 mg/mL benzamide, and 5 μM of Cmpd-1. Ni-affinity resin was added and mixing continued for another 2 h at 4 °C. The Ni-affinity resin was collected by spinning, and washed extensively with Ni wash buffer comprised of 0.1% DDM, 0.03% CHS, 30 mM Hepes, pH 7.8, 800 mM NaCl, 10% glycerol, 5 mM imidazole, and 5 μM of Cmpd-1. The protein was eluted from Ni-affinity resin by the Ni wash buffer with 200 mM imidazole, and loaded onto an anti-Flag M1 affinity column with the addition of 2.5 mM CaCl₂. The FLAG column was then washed extensively with FLAG wash buffer comprised of 0.1% DDM, 0.03% CHS, 30 mM Hepes, pH 7.8, 800 mM NaCl, 5 μM of Cmpd-1 and 2.5 mM CaCl₂. The detergent DDM was then gradually exchanged over 1 h into a buffer with 0.01% LMNG, 0.001% CHS, 30 mM Hepes, pH 7.8, 800 mM NaCl, and 5 μM of Cmpd-1. The receptor was eluted from the FLAG column using the same buffer but without CaCl₂ and containing 200 μM FLAG peptide and 5 mM EDTA. The elution sample was concentrated and loaded onto a SEC column (Superdex 200) with the buffer 0.01% LMNG, 0.001% CHS, 30 mM Hepes, pH 7.8, 800 mM NaCl, and 5 μM of Cmpd-1. The major peak fractions were combined and concentrated for crystallization and the ligand was added up to 20 μM final concentration.

Crystallization. We performed extensive LCP crystallization trials for A_{2A}R-T4L, A_{2A}R-mT4L, and A_{2A}R-BRIL following similar conditions as previous reported (8, 14). No crystal or only poorly diffracting crystals were obtained even after extensive optimization. We obtained crystals that diffracted beyond 3.5 Å resolution by vapor-phase diffusion. The crystals grew in 0.045 M Mes, pH 6.5, 0.045 M MgCl₂, 28% (vol/vol) PEG400, 5% (vol/vol) Jeffamine M-600 (pH 7.0) at 20 °C and were harvested by flash-freezing directly into liquid nitrogen. All of the LCP and vapor-phase diffusion crystallization trials were performed by Gryphon LCP robot (Art Robbins Instruments).

Data Collection and Structure Determination. Data collection was performed using the beamline 23-ID of GM/CA@APS at the Advanced Photon Source. Microbeams of 10 or 20 μm diameter were used to acquire all diffraction data. Owing to radiation damage, only 5–20° of rotation data were collected from each crystal. All data were processed with the HKL2000 package (24). A 3.5-Å dataset was obtained by merging diffraction data from 20 crystals. The space group was determined to be P4₁2₁2. Molecular replacement was performed using the program Phaser in the CCP4 package (25), with separate A_{2A}R and BRIL chain from A_{2A}R-BRIL-ZM241385 structure (PDB ID code 4E1Y) as the search model. Iterative model-building and structural refinement

were performed using COOT (26) and Refmac5 (27), respectively. The quality of the structure was assessed using MolProbity (28). Data processing and structure refinement statistics are shown in Table S1.

Ligand Optimization. Using Percepta 2014 software, Cmpd-1 was predicted to have a pK_a of ~9 and thus under physiological conditions will be protonated (ACD/Percepta; Advanced Chemistry Development, Inc.). The Percepta software predicted that the NH moiety of the linker group that is closest to the aminotriazole ring is the most basic. This protonated form of the ligand in the RX structure was then submitted for a quantum mechanical (QM) optimization calculation using Jaguar version 8.4 (29). The QM calculation was performed using the B3LYP density functional theory (DFT) method with the 6-31G** basis set and the Poisson–Boltzmann Finite water solvation model, and XYZ Cartesian constraints were applied to all of the heavy atoms of the ligand with the exception of the linker region to help relieve apparent intramolecular strains within the linker region. To be noted, a methoxy group is usually found to be coplanar with the aromatic ring of methoxyphenyl, because this allows for overlap between the oxygen atom nonbonding orbital and the aromatic π system; this is not possible, however, for Cmpd-1, because steric clashes with the protein prevent it from assuming a coplanar configuration with the ring. Although unusual, examples of displacement of the methoxy group away from coplanarity have been observed previously (compare PDB ID codes 2bkt and 2bks). Further, a 5° incremental rigid-torsion QM scan of the methoxy group (using the same version of Jaguar, solvation model, DFT, and basis set as described above) revealed that the orientation of the methoxy group in our structure incurs less than +2.5 Kcal/mol energy penalty relative to the configuration where the methoxy is coplanar.

Binding assay. Ligand-binding studies for the adenosine receptors were done in membranes pretreated with adenosine deaminase prepared from HEK293 cells. For inhibition of binding to the human A_{2A}R, membranes were incubated for 60 min with [³H]-ZM241385 (0.4 nM) at 25 °C (30). The reaction was terminated by rapid filtration over polyethyleneimine-treated glass-fiber filters and non-specific binding determined by 10 μM 5'-*N*-ethylcarboxamido adenosine (NECA). For inhibition of binding to the human A₁R, membranes were incubated as above with 0.15 nM [³H]-DPCPX, and nonspecific binding was defined with 100 μM 2-chloroadenosine.

Functional assay. The ability to inhibit A_{2A}R function was determined in CHO cells expressing human A_{2A} receptor. Cells were preincubated for 60 min with the compound, and then incubated for a further 60 min in the presence of a submaximal concentration (100 nM) of the agonist CGS21680 in buffer containing 10 μM rolipram. Changes in cAMP levels were determined using the CisBio HTRF Kit.

- de Lera Ruiz M, Lim YH, Zheng J (2014) Adenosine A_{2A} receptor as a drug discovery target. *J Med Chem* 57(9):3623–3650.
- Shook BC, Jackson PF (2011) Adenosine A_{2A} receptor antagonists and Parkinson's disease. *ACS Chem Neurosci* 2(10):555–567.
- Pinna A, Wardas J, Simola N, Morelli M (2005) New therapies for the treatment of Parkinson's disease: Adenosine A_{2A} receptor antagonists. *Life Sci* 77(26):3259–3267.
- Milne GR, Palmer TM (2011) Anti-inflammatory and immunosuppressive effects of the A_{2A} adenosine receptor. *Sci World J* 11:320–339.
- Bara-Jimenez W, et al. (2003) Adenosine A_{2A} receptor antagonist treatment of Parkinson's disease. *Neurology* 61(3):293–296.
- Michel A, Downey P, Nicolas JM, Scheller D (2014) Unprecedented therapeutic potential with a combination of A_{2A}/NR2B receptor antagonists as observed in the 6-OHDA lesioned rat model of Parkinson's disease. *PLoS One* 9(12):e114086.
- Lebon G, Edwards PC, Leslie AG, Tate CG (2015) Molecular determinants of CGS21680 binding to the human adenosine A_{2A} receptor. *Mol Pharmacol* 87(6):907–915.
- Liu W, et al. (2012) Structural basis for allosteric regulation of GPCRs by sodium ions. *Science* 337(6091):232–236.
- Congreve M, et al. (2012) Discovery of 1,2,4-triazine derivatives as adenosine A_{2A} antagonists using structure based drug design. *J Med Chem* 55(5):1898–1903.
- Hino T, et al. (2012) G-protein-coupled receptor inactivation by an allosteric inverse-agonist antibody. *Nature* 482(7384):237–240.
- Xu F, et al. (2011) Structure of an agonist-bound human A_{2A} adenosine receptor. *Science* 332(6027):322–327.
- Doré AS, et al. (2011) Structure of the adenosine A_{2A} receptor in complex with ZM241385 and the xanthines XAC and caffeine. *Structure* 19(9):1283–1293.
- Lebon G, et al. (2011) Agonist-bound adenosine A_{2A} receptor structures reveal common features of GPCR activation. *Nature* 474(7352):521–525.
- Jaakola VP, et al. (2008) The 2.6 angstrom crystal structure of a human A_{2A} adenosine receptor bound to an antagonist. *Science* 322(5905):1211–1217.
- Caffrey M (2015) A comprehensive review of the lipid cubic phase or in meso method for crystallizing membrane and soluble proteins and complexes. *Acta Crystallogr F Struct Biol Commun* 71(Pt 1):3–18.
- Caffrey M, Cherezov V (2009) Crystallizing membrane proteins using lipidic mesophases. *Nat Protoc* 4(5):706–731.
- Thorsen TS, Matt R, Weis WI, Kobilka BK (2014) Modified T4 lysozyme fusion proteins facilitate G protein-coupled receptor crystallogensis. *Structure* 22(11):1657–1664.
- Chun E, et al. (2012) Fusion partner toolchest for the stabilization and crystallization of G protein-coupled receptors. *Structure* 20(6):967–976.
- Russo Krauss I, Merlino A, Vergara A, Sica F (2013) An overview of biological macromolecule crystallization. *Int J Mol Sci* 14(6):11643–11691.
- Ballesteros JA, Weinstein H (1995) Integrated methods for the construction of three-dimensional models and computational probing of structure-function relations in G protein-coupled receptors. *Methods Neurosci* 25:366–428.
- Palczewski K, et al. (2000) Crystal structure of rhodopsin: A G protein-coupled receptor. *Science* 289(5480):739–745.
- Chien EY, et al. (2010) Structure of the human dopamine D₃ receptor in complex with a D₂/D₃ selective antagonist. *Science* 330(6007):1091–1095.
- De Zwart M, et al. (1999) Potent antagonists for the human adenosine A_{2B} receptor. Derivatives of the triazolotriazine adenosine receptor antagonist ZM241385 with high affinity. *Drug Dev Res* 48:95–103.
- Otwinowski Z, Minor W (1997) Processing of X-ray diffraction data collected in oscillation mode. *Methods Enzymol* 276:307–326.
- McCoy AJ, et al. (2007) Phaser crystallographic software. *J Appl Cryst* 40(Pt 4):658–674.
- Emsley P, Lohkamp B, Scott WG, Cowtan K (2010) Features and development of Coot. *Acta Crystallogr D Biol Crystallogr* 66(Pt 4):486–501.
- Murshudov GN, Vagin AA, Dodson EJ (1997) Refinement of macromolecular structures by the maximum-likelihood method. *Acta Crystallogr D Biol Crystallogr* 53(Pt 3):240–255.
- Chen VB, et al. (2010) MolProbity: All-atom structure validation for macromolecular crystallography. *Acta Crystallogr D Biol Crystallogr* 66(Pt 1):12–21.
- Bochevarov AD, et al. (2013) Jaguar: A high-performance quantum chemistry software program with strengths in life and materials sciences. *Int J Quantum Chem* 113(18):2110–2142.
- Palmer TM, Poucher SM, Jacobson KA, Stiles GL (1995) 125I-4-[2-[7-amino-2-[furyl][1,2,4]triazolo[2,3-a][1,3,5] triazin-5-yl-amino]ethyl]phenol, a high affinity antagonist radioligand selective for the A_{2A} adenosine receptor. *Mol Pharmacol* 48(6):970–974.